Large deformation of magnetic hydrogels subject to different magnetic field types

Qimin Liu[1,2], Lewei He[3], Xin Ye[4], Mokarram Hossain[5], Elvis Chun-sing Chui[4,*], Xingyu Zhang[6,*]

[1]*School of Civil Engineering and Architecture, Wuhan University of Technology, Wuhan 430070, P. R. China*

[2]*Hubei Key Laboratory of Roadway Bridge & Structure Engineering , Wuhan, 430070, P. R. China*

[3]*School of Software, South China Normal University, Guangzhou 510631, P. R. China*

[4] *Department of Orthopaedics and Traumatology, Faculty of Medicine, The Chinese University of Hong Kong, Hong Kong 999077, P. R. China*

[5] *Zienkiewicz Institute for Modelling, Data and AI, Swansea University, Swansea, SA1 8EN, United Kingdom*

[6]*School of Mathematics, Statics and Mechanics, Beijing University of Technology, Beijing, P. R. China*

*Corresponding authors

Elvis Chun-sing Chui	elvis_chui@cuhk.edu.hk	Tel: (852) 35052721
Xingyu Zhang	xingyu0711@bjut.edu.cn	Tel: (86) 17717865437

ABSTRACT: Soft materials that can dynamically reconfigure its morphology upon interaction with environment or perceptions of information is currently thriving. Among these materials, magnetic hydrogels offer great opportunities for novel applications, particularly within biomedical field. However, the design of magnetic hydrogels is rather complicated since (i) it concurrently combines large deformation, magneto-active response and solvent diffusion, and (ii) the relationship remains unclear between the hydrogel performance and various magnetic field types, including uniform, nonuniform, and low-frequency alternating magnetic fields. Herein, a multiphysics model is developed to characterize the coupled processes of hydrogel magnetization, solvent diffusion and large deformation of the hydrogel, based on a general thermodynamically consistent framework. In particular, the magnetic boundary conditions are specified by solving the Laplace's equation for the magnetic scalar potential if a nonuniform magnetic field is imposed. Various case studies are conducted to investigate the influences of magnetic permeability, field distribution coefficients, and hydrogel-magnet distance on the hydrogel performance. The numerical results show that the morphology of the hydrogel can be rapidly tailored and the way it deforms changes significantly depending on the magnetic field type used. Additionally, the hydrogel elongates along the field direction under a uniform magnetic field, while it shrinks when a nonuniform magnetic field is applied. The present multiphysics model may provide theoretical guidance for optimal design and control of the magnetic hydrogel system.

Keywords: Magnetic hydrogel; multiphysics model; magnetic field types; large deformation

1. Introduction

Soft matter that can dynamically reconfigure its morphology upon interaction with environment or perceptions of information is currently thriving. Stimuli-responsive polymers, particularly magneto-active polymers, have become increasingly popular in biomedical and bioengineering fields [1-3], due to their ability to achieve specific multi-functional properties, such as tunable mechanical characteristics and the capacity for complex, re-programmable shape morphology at different length scales [4, 5]. Generally, magneto-active polymers are categorized into magnetic elastomers and hydrogels, both of which consist of a soft polymeric matrix embedded with magnetic particles, having their common properties in many cases. For instance, they can change their shape and stiffness in response to a magnetic field, and their mechanical behaviors can be remotely tailored without physical contact. However, magnetic hydrogels are typically softer than magnetic elastomers, due to the presence of a liquid phase [6-8]. Elastomers often work in air environment that is not surrounded by liquid, and they are commonly used in engineering applications, such as dampers and grippers. On the other hand, magnetic hydrogels, with their hydrophilic nature, are generally used in solvent environments for biomedical applications, due to their easy synthesis, excellent biocompatibility, and biodegradability [9].

As a soft magnetic composite, the performance of magnetic hydrogel is closely linked to its constituents. Basically, the hydrogel matrix is insensitive to the external magnetic field, such that the overall magnetization of the magnetic hydrogel largely relies on the magnetizability of the magnetic particles within it. Usually magnetic particles with micro- or nano-sized are mostly employed, since the particles show a null magnetization without

hysteresis under a null magnetic field. Due to their soft nature, rapid actuation, excellent controllability, and good compatibility in biological environments, magnetic hydrogels have been potentially used in biomedical engineering (e.g. tissue engineering, drug release and delivery systems) [3, 10], soft matter engineering (e.g. soft robotics, soft morphing devices, artificial skins/interfaces) [11-14], as well as in the design of intelligent structures and systems with dynamic properties [15].

A notable advantage of magnetic hydrogels is their ability to be remotely activated by external magnetic fields, making them a robust and prominent method for actuating objects, particularly on a relatively small scale. To comprehend how magnetic hydrogels behave under an external magnetic field, numerous experimental studies on their deformable behaviors have been extensively conducted. These studies have found that magnetic hydrogels may deform under different magnetic field types or due to absorbing solvent from the surrounding. [16-20]. (I) *Under a uniform static magnetic field*, the magnetic moment of any magnetic particle is maintained along its easy-axis direction and thus randomly distributed, thereby the macroscopic magnetization of the magnetic hydrogel is null. Once an uniform field is imposed, the magnetic hydrogel may be magnetized through Néel or Brownian relaxation mechanisms [21]. This leads to the initiation of particle-particle interactions, causing the particles to attract or repel each other. As the particles are often tightly attached to the polymer chains by covalent bonding as the crosslinker [22], their movements induce an overall macroscopic deformation of the hydrogel. (II) *Under a nonuniform static magnetic field*, the magneto-induced deformation may be more pronounced due to the additional contribution from the magnetic field gradient [20]. In addition, the magnetic hydrogel may undergo both movement and

deformation when it is unconstraint [23, 24]. (III) *Under an alternating magnetic field,* the magnetic hydrogels deform with a prescribed frequency if a low-frequency alternating magnetic field is imposed [25]. At relatively high magnetic field frequencies (e.g., several kHz), the magneto-thermal transition occurs due to Néel or Brownian relaxation. Furthermore, if the hydrogel is also temperature-sensitive, e.g. PNIPAAm-type hydrogels, the generated heat can stimulate a phase change in the magnetic hydrogel [9]. (IV) *By* absorbing *solvent from the surrounding*, hydrogels are essentially hydrophilic. That means, when it is placed in a solvent surrounding, the hydrogel may undergo a significant volume change. Concurrently, the deformation may be further changed when a magnetic field is additionally exerted [26].

The deformation of magnetic hydrogels is highly dependent on the multiphysics coupling process of magnetization, solvent diffusion, and large deformation. According to the latest literature review, most existing works on deformable behaviors were experiment-based and thus time-consuming, and they may not fully capture all the effects on the performance of magnetic hydrogels. Alternatively, theoretical modeling is expected to provide a more comprehensive understanding of the performance of magnetic hydrogels. The inchoate theoretical works mainly focused on the magneto-mechanical behavior of the magnetic hydrogel, and they are categorized based on different length scales. At the macroscopic scale, the magnetic hydrogel was regarded as a continua with incompressible property [27]. Recently, the macroscopic magneto-mechanical models have been extensively developed, where linear or nonlinear elasticity was fully coupled with the Maxwell equations, and the constitutive relations were derived based on the second law of thermodynamics [7, 27-30]. At the mesoscopic scale, the polymeric network is considered

as an elastic continuum, while the embedded magnetic particles were regarded as dipoles. This approach allows for the detailed study of the effects of particle shape and spatial distribution on the deformation of magnetic hydrogels [31, 32]. To capture more microscopic details, various microscopic models in two and three dimensions have been formulated, considering the interaction between individual polymer chains and magnetic particles [21, 33]. Additionally, a bridge approach has been proposed among different length scales, such as detailed microscopic simulations and coarse-grained mesoscopic models [34]. It is noted that, in magneto-mechanical models, the hydrogel often works in the air surrounding and deforms with a constant volume. However, when considering the magnetic hydrogel in a solvent surrounding, solvent diffusion is necessarily considered, characterized by a chemical field. In other words, apart from the magneto-mechanical field, the chemical field needs to be coupled with the magneto-mechanical field.

A further literature search shows that few theoretical models were developed for the performance of magnetic hydrogel in a solvent surrounding. To the best of author's knowledge, Filipcsei *et al*. [35] may be the first to investigate the swelling of the magnetic hydrogel that was submerged in a solvent surrounding and placed in a uniform magnetic field. However, it is unable to properly characterize the deformable behavior of the magnetic hydrogel, as the predicted swelling deformation of the hydrogel is independent of the magnetic field direction. To address the limitation, by the conservation laws and the second law of thermodynamics, a magneto-chemo-mechanical model was developed to simulate the responsive behavior of the magnetic hydrogel subject to various stimuli. This model was validated and then well performed for the responsive behavior of the magnetic hydrogel [36, 37]. Recently, the multiphysics model was extended with the additional

effect of viscosity for the hydrogel responses at the short and long time scales when subjected to a uniform magnetic field [38]. The multiphysics model was also extended to study the responsive behavior of magnetic- and dual magnetic-pH-sensitive hydrogels with the coupled magneto-chemo-electro-mechanical coupled effects [39, 40]. More recently, the inhomogeneous large deformation of magneto-thermal sensitive hydrogels-based composite structures under external stimuli was investigated, where the total energy due to magnetization of all magnetic dipoles was equaled to the heat energy due to the temperature change [41]. These advancements in theoretical modeling not only enhance our understanding of the behavior of magnetic hydrogels but also pave the way for the design and development of innovative applications based on these materials.

To date, the deformations of the magnetic elastomers and hydrogels have been experimentally and theoretically investigated. Various magnetic field types are used to drive the hydrogel deformation, such as uniform and nonuniform static fields, and low-frequency alternating magnetic fields. Among most, the deformation in a uniform magnetic field is frequently simulated, probably because the magnetic boundary conditions for a uniform magnetic field are easily specified through the definition of magnetic scalar potential at the boundary. To generate a nonuniform magnetic field, a permanent magnet or an electromagnet is commonly used, and their geometries are necessarily incorporated in the finite element models [42-44], which may require much time for the numerical computation. Hence, an efficient way to simulate the magnetic field is required for the complicated multiphysics problems. Furthermore, literature shows that a comprehensive study is not currently reported for the impact of various magnetic field types on the deformable behaviors of magnetic hydrogels.

Herein, the deformation of magnetic hydrogel is thoroughly examined using a multiphysics model under various magnetic field types. The work is driven by the growing applications of magnetic hydrogels in biomedicine, such as soft robots, pulsatile drug release, and microfluidic valves under different magnetic field types [12, 25, 45], which necessitate a comprehensive understanding of the magneto-induced large deformation of hydrogels. The model integrates magneto-chemo-mechanical effects and accounts for the significant deformation of the hydrogel. The governing equations are derived from mass and force balances, while the constitutive relations are based on the second law of thermodynamics, considering the influence of magnetic fields, chemical potential, and large deformation. Additionally, three physicochemical reactive mechanisms are characterized, including hydrogel magnetization, solvent diffusion, and large deformation. Furthermore, the study comprehensively investigates the deformation of hydrogels under different magnetic field types and various magnetic permeabilities, hydrogel-magnet distances, field distribution coefficients.

2. Theory

In this section, a thermodynamically consistent framework is theoretically developed for magnetic hydrogels with magneto-chemo-mechanical coupled field, where the governing equations are derived based on conservations of mass and linear momentum, and the constitutive equations are obtained by the second law of thermodynamics. Moreover, the boundary and initial conditions are given for the mathematical model, followed by the model implementation with finite element method. In general, the model can be developed in a reference configuration with Lagrangian form or in a current configuration with Eulerian form. In the present model, the Lagrangian form is selected, since the Eulerian

one may require a moving mesh for the large deformation problems [46]. Additionally, the following assumptions are made in development of the multiphysics model: (I) The magnetic particles are evenly distributed throughout the hydrogel matrix. (II) The hydrogel exhibits macroporous properties, allowing for the diffusivity constant of solvent molecules to remain consistent in both the hydrogel and surrounding solvent. (III) There are no chemical reactions between the hydrogel and solvent species. (IV) Stretching of the polymer chains is a much faster process than migration of solvent molecules, such that the process of local mechanical equilibrium is taken to be instantaneous and we assume local equilibrium by neglecting viscosity [47].

2.1. Governing equations

In the absence of free current, the distributions of magnetic intensity **H** and magnetic induction **B** in reference configuration are described by the Maxwell's equations [27, 30]

$$\nabla \times \mathbf{H} = \mathbf{0}, \qquad \nabla \cdot \mathbf{B} = 0 \tag{1}$$

where $\nabla \times (\bullet)$ and $\nabla \cdot (\bullet)$ are the material curl and divergence operators respectively with respect to Lagrangian coordinate **X**. From Equation (1) for magnetic intensity **H**, it is known that it can be written as the negative gradient of the magnetic scalar potential ψ, namely

$$\mathbf{H} = -\nabla \psi \tag{2}$$

such that the governing equations for the magnetic intensity in Equation (1) and the magnetic boundary conditions in Equation (21) may be expressed by the magnetic potential ψ instead of the magnetic intensity **H** and induction **B**.

To characterize the diffusion of solvent molecules, the conservation law of mass is employed as [48, 49]

$$\dot{C}_s = -\nabla \cdot \mathbf{J}_s + R_s \tag{3}$$

where $C_s(\mathbf{X},t)$ is the concentration of solvent inside the magnetic hydrogel, $\mathbf{J}_s$ is the solvent flux density that enters into the hydrogel across the interface, and R_s is the generation of solvent per unit reference volume per unit time.

With regard to the large deformation of the hydrogel, the conservation of linear momentum is used by [50]

$$\rho_0 \dot{\mathbf{V}}_h = \nabla \cdot \mathbf{P} + \mathbf{f}_b \tag{4}$$

where ρ_0 is the nominal mass density of the polymer matrix, $\mathbf{P}$ is the first Piola–Kirchhoff stress, $\mathbf{V}_h$ is the deformation velocity, and $\mathbf{f}_b$ is the external force density.

2.2. Constitutive relations derived by the second law of thermodynamics

Based on the principles of thermodynamics [29, 50], the increase rate of the free energy density of the hydrogel system is essentially less than the external power caused by the external force, the chemical power resulting from solvent diffusion, and the magnetic power due to hydrogel magnetization, namely

$$\frac{d}{dt}\{\int_{V_0}(W+\frac{1}{2}\rho_0\left|\mathbf{V}_h\right|^2)dv\} \le \underbrace{\int_{S_0}\mathbf{P}\mathbf{N}\cdot\mathbf{V}_h ds+\int_{V_0}\mathbf{f}_b\cdot\mathbf{V}_h dv}_{\text{External power}}+\underbrace{\int_{V_0}\mu_s R_s dv-\int_{S_0}\mu_s\mathbf{J}_s\cdot\mathbf{N}ds}_{\text{Chemical power}}+\underbrace{\int_{V_0}\mathbf{H}\cdot\dot{\mathbf{B}}dv}_{\text{Magnetic power}} \tag{5}$$

where W is the free energy density and μ_s is the chemical potential of solvent.

By the divergence theorem, Equation (5) is rewritten as

$$\int_{V_0} \dot{W} dv + \int_{V_0} (\rho_0 \dot{\mathbf{V}}_h \cdot \mathbf{V}_h) dv \leq \int_{V_0} [(\nabla \cdot \mathbf{P}) \cdot \mathbf{V}_h + \mathbf{P} : \nabla \mathbf{V}_h + \mathbf{f}_b \cdot \mathbf{V}_h + \mu_s R_s - \mu_s \nabla \cdot (\mathbf{J}_s) - \mathbf{J}_s \cdot \nabla \mu_s + \mathbf{H} \cdot \dot{\mathbf{B}}] dv \tag{6}$$

By Equations (3) and (4), we obtain the local form of the free energy imbalance (5), namely

$$\dot{W} \leq \mathbf{P} : \dot{\mathbf{F}} + (\mu_s \dot{C}_s - \mathbf{J}_s \cdot \nabla \mu_s) + \mathbf{H} \cdot \dot{\mathbf{B}} \tag{7}$$

where $\mathbf{F}$ is the deformation gradient, and $\dot{\mathbf{F}} = \nabla \mathbf{V}_h$.

The present magneto-chemo-mechanical coupled system includes three physical fields that are characterized by three independent variables, namely the deformation gradient $\mathbf{F}$, magnetic induction $\mathbf{B}$, and solvent concentration C_s, namely $W = W(\mathbf{F}, \mathbf{B}, C_s)$. Then we have

$$\dot{W} = \frac{\partial W}{\partial \mathbf{F}} : \dot{\mathbf{F}} + \frac{\partial W}{\partial \mathbf{B}} \cdot \dot{\mathbf{B}} + \frac{\partial F}{\partial C_s} \dot{C}_s \tag{8}$$

Substituting Equation (8) into (6), we have the following inequality,

$$(\mathbf{P} - \frac{\partial W}{\partial \mathbf{F}}) : \dot{\mathbf{F}} + (\mathbf{H} - \frac{\partial W}{\partial \mathbf{B}}) \cdot \dot{\mathbf{B}} + (\mu_s - \frac{\partial W}{\partial C_s}) \dot{C}_s - \mathbf{J}_s \cdot \nabla \mu_s \geq 0 \tag{9}$$

Since the independent variables are arbitrary, the coefficient vanishes in any bracket [51]. Additionally, in order to ensure the inequality (8) hold, the solvent flux $\mathbf{J}_s$ is written as the negative gradient of the chemical potential $\nabla \mu_s$ [47]

$$\mathbf{J}_s = -\mathbf{L} \nabla \mu_s \tag{10}$$

where the positive-definite tensor $\mathbf{L} = C_s D_s \mathbf{C}^{-1} / (k_B T)$, D_s is the diffusion coefficient, $\mathbf{C} = \mathbf{F}^T \mathbf{F}$ is the right Cauchy-Green tensor, and $k_B T$ is the temperature in the unit of energy. Then we have the constitutive relations with partial differential form below

$$\mathbf{P} = \frac{\partial W}{\partial \mathbf{F}}, \quad \mathbf{H} = \frac{\partial W}{\partial \mathbf{B}}, \quad \mu_s = \frac{\partial W}{\partial C_s} \tag{11}$$

It is noted that the magnetic intensity $\mathbf{H}$ and the magnetization $\mathbf{M}$ can also be the independent variables, where an augmented free energy is accordingly required by the partial Legendre transformation. For example, if the magnetic intensity $\mathbf{H}$ is used as the independent variable instead of the induction $\mathbf{B}$, an augmented free energy density Ω is necessarily defined [29]

$$\Omega(\mathbf{F}, \mathbf{H}, C_s) = W(\mathbf{F}, \mathbf{B}, C_s) - \mathbf{H} \cdot \mathbf{B} \tag{12}$$

then the constitutive relation (11) is rewritten as

$$\mathbf{P} = \frac{\partial \Omega}{\partial \mathbf{F}}, \quad \mathbf{B} = -\frac{\partial \Omega}{\partial \mathbf{H}}, \quad \mu_s = \frac{\partial \Omega}{\partial C_s} \tag{13}$$

To attain the explicit form of the variables, $\mathbf{P}$, $\mathbf{B}$, and μ_s, a specific free energy density Ω is required. In the present study, the free energy density Ω consists of the elastic free energy density for stretching the polymeric network, the mixing free energy density for the polymer and solvent molecules, and the magnetic free energy density for the magnetization of the hydrogel. If the molecular incompressibility condition is considered, i.e. $1 + v_s C_s = \det(\mathbf{F})$ [47], we have the following specific free energy density [47, 52-54]

$$\Omega = \frac{1}{2}G\left(\mathrm{tr}(\mathbf{F}^T\mathbf{F}) - 3 - 2\ln\left(\det(\mathbf{F})\right)\right) - \frac{J\mu_m}{2}\left((\mathbf{F}^{-T}\mathbf{H})\cdot(\mathbf{F}^{-T}\mathbf{H})\right) + \frac{k_B T}{v_s}\left(v_s C_s \ln\left(\frac{v_s C_s}{1+v_s C_s}\right) + \frac{\chi_H v_s C_s}{1+v_s C_s}\right) + \Pi\left(1 + v_s C_s - \det(\mathbf{F})\right) \tag{14}$$

where G is the hydrogel shear modulus, v_s is the volume per solvent molecule, χ_H is the Flory-Huggins parameter that describes the polymer-solvent interaction, μ_m is the magnetic permeability of the hydrogel that is related to the relative permeability μ_{mr} through $\mu_m = \mu_0\mu_{mr}$, $J = \det(\mathbf{F})$ is the determinant and $J > 0$, and Π is the Lagrange multiplier or the osmotic pressure [47].

According to the constitutive relation (13) and the free energy density (14), the magnetic induction $\mathbf{B}$, the chemical potential μ_s, and the nominal stress $\mathbf{P}$ are respectively given below

$$\mathbf{B} = J\mu_m\mathbf{C}^{-1}\mathbf{H} \tag{15}$$

$$\mu_s = k_B T[\ln(1 - \frac{1}{1+v_s C_s}) + \frac{1}{1+v_s C_s} + \frac{\chi_H}{(1+v_s C_s)^2}] + \Pi v_s \tag{16}$$

$$\mathbf{P} = G(\mathbf{F} - \mathbf{F}^{-T}) - J\Pi\mathbf{F}^{-T} + J\mu_m\mathbf{F}^{-T}\cdot(\mathbf{H}\otimes\mathbf{H})\cdot\mathbf{C}^{-1} - J\mu_m\mathbf{F}^{-T}\cdot[(\mathbf{C}^{-1}\cdot\mathbf{H})\cdot\mathbf{H}]/2 \tag{17}$$

By Equations (2) and (15), the governing equation (1) for the magnetic intensity **H** and induction **B** can be rewritten as a function of magnetic potential ψ only,

$$\nabla\cdot(J\mu_m\mathbf{C}^{-1}\nabla\psi) = 0 \tag{18}$$

2.3. Boundary and initial conditions

To solve the governing equations and their corresponding constitutive relations, it is essential to establish the initial and boundary conditions, which are outlined as follows.

If a uniform magnetic field is applied along the Z-axis, the magnetic boundary conditions at the edge of the cylindrical surrounding are given by

$$\psi\big|_{Z=0}=0,\ \ \psi\big|_{Z=L_Z}=-H_0L_Z,\ \ \frac{\partial\psi}{\partial R}\Big|_{R=0,\,L_R}=0 \tag{19}$$

where R_0 and L_Z are the radius and length of the surrounding, as shown in Figure 2.

If a magnet is placed at the bottom of the magnetic hydrogel, a nonuniform magnetic field is created and the magnetic boundary condition for the magnetic scalar potential ψ at the edge of the solvent is given as

$$\psi=\psi(\mathbf{X},t) \tag{20}$$

this boundary condition can be reconstructed from the original magnetic field along the vertical line $R=0$, which will be elucidated in Subsection 4.2.

At the hydrogel-surrounding interface $\partial\beta_0$, the magnetic parameters are required to meet the jump conditions below [27]

$$\mathbf{N}\times[[\mathbf{H}]]=\mathbf{0},\quad \mathbf{N}\cdot[[\mathbf{B}]]=0 \tag{21}$$

where $\mathbf{N}$ is the unit normal vector, and the double bracket $[[\square]]$ is a quantity jump across the surface from the inside to outside of the material. For simplicity, the magnetic boundary conditions for the magnetic intensity **H** and **B** at the hydrogel-surrounding interface $\partial\beta_0$ are written in the form of magnetic scalar potential ψ,

$$[[\psi]]=0,\ \ \mu_{mr}\frac{\partial\psi}{\partial N}\Big|_{\partial\beta_0^+}=\frac{\partial\psi}{\partial N}\Big|_{\partial\beta_0^-} \tag{22}$$

and the chemical and mechanical boundary conditions at the interface $\partial\beta_0$ are given below,

$$\mu_s=\mu_s^*,\ \ \mathbf{P}\cdot\mathbf{N}=\mathbf{T}_a+\mathbf{T}_m \tag{23}$$

where μ_s^* represents the chemical potential of the surrounding solvent and $\mu_s^* = 0$. $\mathbf{T}_a$ is the mechanical traction and $\mathbf{T}_m = \mathbf{P}_m \cdot \mathbf{N}$ is the magnetic traction, here the Maxwell stress $\mathbf{P}_m$ is given by,

$$\mathbf{P}_m = \mathbf{F}^{-T}(\mathbf{H} \otimes \mathbf{B}) - (\mathbf{H} \cdot \mathbf{B})\mathbf{F}^{-T}/2 \tag{24}$$

Regarding the initial conditions, they are written as

$$\mu_s = \mu_{s0}, \quad \mathbf{P} = \mathbf{0} \tag{25}$$

where the initial chemical potential μ_{s0} is obtained via Equations (16) and (17) by setting the stress $\mathbf{P} = \mathbf{0}$ [55].

Currently, the multiphysics model has been theoretically formulated for the magnetic hydrogel submerged in the surrounding solvent and subjected to magnetic-chemo-mechanical coupled fields. It includes the magnetostatic equation (18), the mass conservation equation (3), and the mechanical equilibrium equation (4). Additionally, the specific free energy density is provided by Equation (14), and the constitutive relations are achieved through Equations (10) and (15) ~ (17).

3. Model implementation

The solution to the initial/boundary value problem entails dealing with the vector field of location $\mathbf{x}(\mathbf{X}, t)$, the scalar fields of magnetic potential $\psi(\mathbf{X}, t)$, and the chemical potential of solvent $\mu_s(\mathbf{X}, t)$. These factors are interconnected and evolve simultaneously over time. To derive the weak forms of the governing equations, we utilize a set of test functions, $\delta\mathbf{x}$, $\delta\psi$, and $\delta\mu_s$, that meet the necessary integrability criteria. Multiplying Equation (3) by $\delta\mu_s$, integrating over V_0, and by the divergence theorem, we have [55]

$$\int_{\Omega_0} \dot{C}_s \delta\mu_s dV_0 = \int_{\Omega_0} \mathbf{J}_s (\nabla \delta\mu_s) dV_0 - \int_{\partial\Omega_0} (\mathbf{J}_s \cdot \mathbf{N}) \delta\mu_s dS_0 + \int_{\Omega_0} R_s \delta\mu_s dV_0 \tag{24}$$

where Ω_0 is the computational domain covering both the hydrogel and surrounding. In a similar way, the weak forms of the governing equations for the magnetization and the mechanical deformation are given by [29]

$$\int_{\Omega_0} (J\mu_m \mathbf{C}^{-1} \nabla\psi) \nabla(\delta\psi) dV_0 = \int_{\partial\Omega_0} B_N (\delta\psi) dS_0 \tag{25}$$

$$\int_{\beta_0} \rho_0 \dot{\mathbf{V}}_h \delta\mathbf{x} dV_0 = -\int_{\beta_0} \mathbf{P} : \delta\mathbf{F} dV_0 + \int_{\partial\beta_0} \mathbf{T} \cdot \delta\mathbf{x} dS_0 + \int_{\beta_0} \mathbf{f}_b \cdot \delta\mathbf{x} dV_0 \tag{26}$$

where $B_N = \mathbf{B} \cdot \mathbf{N}$ is the magnetic induction along the unit normal and $\mathbf{T} = \mathbf{P} \cdot \mathbf{N}$ is the nominal traction on the hydrogel surface.

The above weak forms from (25) to (27) constitute the magneto-chemo-mechanical coupled system, which adequately describes the field evolution. These equations can be directly implemented into the finite element software, COMSOL Multiphysics, by the weak form partial differential equations (PDEs) module. Alternatively, the equations and the corresponding constitutive equations can be implemented with three interfaces in COMSOL: (I) PDE interface adopted for the solvent diffusion, (II) AC/DC interface utilized for the distributive magnetic field, as well as (III) Solid mechanics module used for large deformation of the hydrogel. The numerical implementation in COMSOL is illustrated in Figure 1, and the solving procedure is tabulated in Table 1 below.

The computational domain encompasses both the hydrogel and its surrounding media, which is discretized into quadrilateral elements. Computational results for different mesh sizes are compared to ensure the convergence of the numerical solutions, i.e. independent of the element size, as seen from Subsection 4.1.

4. Results and discussion

In this section, responsive behaviors of magnetic hydrogels are investigated in detail, when subjected to different magnetic field types, including uniform, nonuniform, and low-frequency alternating magnetic fields.

4.1. Deformation in a uniform magnetic field

In the present study, a cylindrical magnetic hydrogel in its dry state is initially placed in a surrounding solvent, and then it gradually swells to a certain volume. Subsequently, a uniform magnetic field created by a pair of electromagnets is imposed, causing the hydrogel to deform along the field direction. Due to the difference in magnetic permeability between the magnetic hydrogel and the solvent, the magnetic field may undergo an abrupt variation at the hydrogel-solvent interface. Therefore, the computational domain of the solvent is considered to obtain a more accurate solution, as depicted in Figure 2. The bottom of the hydrogel is fixed in the *Z*-axial direction during its deformation. For comparison, additionally case studies are conducted, where the dry hydrogel is placed in the solvent and the magnetic field is initially applied. Since the geometry of the hydrogel and the applied magnetic field exhibits axial symmetry, a two-dimensional (2D) transient study is conducted to investigate the hydrogel deformation due to chemical swelling and magnetic stimulus. The relevant input parameters are: the hydrogel radius $r = 2$ mm, hydrogel length $l_z = 4$ mm, shear modulus $G = 40$ kPa (a representative value for hydrogel) [47], Flory-Huggines parameter $\chi_H = 0 \sim 1.2$ (1.0 is adopted) [47], volume per solvent molecule $v_s = 6.02 \times 10^{-5}$ m^3/mol [47], diffusion constant of solvent $D_s = 1 \times 10^{-7}$ m^2/s, and magnetic permeability $\mu_{mr} = 2$, the applied magnetic field

$H_0 = 300\text{kA/m}$, as well as the surrounding size $R = nr$ and $L_Z = nl_z$, n will be obtained by the following analysis. For the transient study, the total computational time is t = 150 s with every timestep of 0.5s. Unless otherwise stated, the inputs for the present numerical simulation follow the above data.

Usually the magnetic hydrogel works in an infinite non-magnetic surrounding, however, it is time-consuming to consider an infinite space when using a standard finite element method. As an alternative, an appropriate surrounding domain is selected by numerically studying the influences of the surrounding sizes on time evolution of the displacement along the magnetic field direction w at the upper side of the magnetic hydrogel, as shown in Figure 3(a). It is obvious that the variation of hydrogel deforms in two stages. The first stage is the free swelling of hydrogel without any magnetic effect when the time $t \le 100\text{s}$, and it is found that the all the deformation patterns for different surrounding sizes R follow the same profile. Because the solvent diffusion and hydrogel swelling at this stage are governed by the chemo-mechanical coupled field, and both the chemical and mechanical boundary conditions are imposed at the hydrogel boundary, leading to the same deformation independent of the surrounding size. Afterwards, the displacements w increase with increasing surrounding radius R from 5r to 7.5r, 10r, 12.5r and 15r. For example, the displacement along the field direction w is about 0.836 mm, when $R = 5r$, and it then becomes 0.888 mm if $R = 7.5r$, 0.907 mm if $R = 10r$. However, if the surrounding radius R increases further from 12.5r to 15r, no significant increase is found in the displacement w. Further, the number of computational elements increases significantly from 22861 to 49694. Therefore, the surrounding size $R = 12.5r$ is used for

the subsequent analysis, with a consideration of the balance between the computational accuracy and cost.

For selection of an appropriate mesh size, a mesh independent study is carried out, in which the displacements at the right point of the upper side of the hydrogels are numerically compared with different maximum mesh sizes L_{elem}, as shown in Figure 3(b). With the decrease of the maximum element size L_{elem}, the vertical displacement w continuously decreases and it eventually converges, since there is no noticeable variation for the deformations when $L_{elem} = 0.5$ mm and 0.2 mm. As such, the element size of 0.5 mm is adopted for the following simulations, since the computational time decreases about 5 times compared with the case of $L_{elem} = 0.2$ mm.

Figure 4 shows the influence of the external magnetic intensity H_0 on variation of the displacement u along the transverse direction and displacement w along the field direction against the time t when subjected to varying relative magnetic permeabilities μ_{mr}. As observed from the figures, the horizontal displacement u decreases with increasing magnetic intensity H_0, and the displacement u further decreases with the increase of the magnetic permeability μ_{mr}, as seen in Figure 4(a), (c), and (e). It also shows that the hydrogel swells at the first 100s due to imbalance of the chemical potentials between the exterior and interior of the hydrogel. Without a magnetic field, the hydrogel continuously swells until an equilibrium state is reached, where the chemical potential of the hydrogel equals with that of the surrounding solvent. Additionally, it is also found that the hydrogel shrinks along the horizontal or the transverse direction after the uniform magnetic field is applied at t =100 s. As illustrated in Figure 4(b), (d), and (e), it is obvious that the hydrogel elongates along the field direction (i.e. Z-axis). With the increase of the magnetic intensity

H_0 from 0 to 300 kA/m, the deformation also increases and hydrogel deformation is nonlinear with the magnetic intensity H_0. For example, when the field H_0 increases from 0 to 100 kA/m and $t = 150\text{s}$, the hydrogel elongates about 0.03 mm, and then it increases up to 0.11 mm and 0.26 mm, respectively, when H_0 increases from 100 to 200 kA/m and then 300 kA/m, as shown in Figure 4(d). It is also noted that the hydrogel can further deform with the increasing magnetic permeability μ_{mr}, because the larger permeability means the larger magnetic force exerted on the hydrogel surface.

Figure 5 demonstrates the time evolutions of the displacement u along the transverse direction and displacement w along the field direction, where the external magnetic intensity H_0 is applied at the initial stage. As seen from the figures, the horizontal displacement u decreases with increasing magnetic intensity H_0, where the increasing rate becomes larger. It is interesting that the displacement u decreases to a negative value and then increase progressively to a positive one when the magnetic field $H_0 = 200$ and 300 kA/m. The hydrogel deformation is dependent on the chemical swelling and the magnetic effect. The chemical swelling is isotropic that induce the expansion of the hydrogel along any direction, while the magnetic effect contributes to the elongation of the hydrogel along the field direction and the contraction along the transverse direction. As such, the deformation profile along the transverse direction is associated with the competition between the chemical and magnetic effects. When the external magnetic field H_0 is small, i.e. 0 and 100 kA/m, the chemical effect is dominant, such that the hydrogel displacement u is always positive. However, when the external magnetic field H_0 is large, i.e. 200 and 300 kA/m, the magnetic effect is dominant at the stage of $t \le 2$ s when only few solvent molecules diffuse into the hydrogel. Therefore, the hydrogel contracts along the transverse

direction. However, the solvent gradually diffuses into the hydrogel with the increasing time t, which expand the hydrogel along the transverse direction, making the displacement u becomes positive and then increases progressively. Regarding the hydrogel displacement w shown in Figure 5(b), it increases with increasing time t, and it further enlarges with the increase of the external magnetic field H_0. Moreover, it is found that the hydrogel initially elongates at a larger speed if the magnetic field H_0 increases, which is different from the phenomenon shown in Figure 4.

For further investigation of the deformable behavior of the magnetic hydrogel, the contours of the hydrogel deformation are illustrated in Figure 6, where the black line represents the original geometry of the hydrogel. As observed from the figure, the hydrogel initially swells from the boundary to the interior location, and the displacement difference between the boundary and the interior location becomes smaller. After the free swelling process (i.e. $t > 100\text{s}$), the hydrogel deforms driven by the chemical and magnetic coupled fields. The hydrogel suddenly elongates along the field direction and shrinks along the transverse direction once an external magnetic field is imposed.

Figure 7(a) is plotted for the spatial distribution of the non-dimensional magnetic intensity $H_Z^* = H_Z / H_0$ along the vertical line at the coordinate $r = 0$ across the surrounding solvent and the magnetic hydrogel. The non-dimensional magnetic intensity H_Z^* remains about 1 when the non-dimensional coordinate $Z^* = Z / L_Z$ increases from 0 to around 0.3, indicating that the external magnetic field is not perturbed as the hydrogel is far from the hydrogel-surrounding interface. If the coordinate Z^* gradually rises, the magnetic intensity H_Z^* rises linearly and then drastically until it reaches a maximum. Subsequently, a sharp decrease occurs in H_Z^*, and then it increases to another maximum at

the center of the hydrogel. The magnetic field distribution may be explained through the following reasons, (I) the different magnetic permeabilities among the hydrogel and the surrounding, and (II) the normal part of the magnetic intensity discontinuously goes through the material boundary based on the magnetic boundary condition (21). Moreover, the figures also demonstrate the hydrogels extend more in the field direction with the increase of H_Z^*. Furthermore, it is also noted from the inset that the magnetic intensity H_Z^* is tangential to the lateral side of the hydrogel, and it is continuously across the lateral side, due to the condition (21). Figure 7(b) is visualized to demonstrate the spatial distribution of the non-dimensional magnetic induction $B_Z^* = B_Z / (\mu_0 H_0)$ along the vertical line at the coordinate $r = 0.5r_0$ across the surrounding solvent and the magnetic hydrogel. The non-dimensional magnetic intensity B_Z^* remains about 1 when the non-dimensional coordinate Z^* is less than 0.3. When the coordinate Z^* further increases, the magnetic induction B_Z^* increases drastically until it reaches a maximum. Different from the distribution of magnetic intensity H_Z^*, the magnetic induction B_Z^* is continuously across the upper and bottom sides of the hydrogel-surrounding interface based on the boundary condition (21), stating that the normal component of the magnetic induction continuously crosses the material boundary, as also seen in the inset of the figure.

4.2. Deformation in a nonuniform magnetic field

In this subsection, the deformable behavior of a cylindrical magnetic hydrogel is investigated in a nonuniform magnetic field, as shown in Figure 8. Initially, the hydrogel lies at its dry state and no magnetic field is applied, such that the hydrogels can freely swell in about 100 s to approach an equilibrium state. After that, a nonuniform magnetic field

created by an electromagnet is imposed vertically at the bottom of the surrounding edge, where L_{hm} is the hydrogel-surrounding distance.

For simulation of the magneto-chemo-mechanical coupled behavior, the magnetic boundary conditions $\psi = \psi(\mathbf{X}, t)$ at the surrounding edge is necessarily required and listed here, based on the work of Afkhami *et al* [56]. Before inserting the magnetic hydrogel into the solvent, the maximum magnetic field occurs at the surface of the electromagnet, and it decays away along the *Z*-axial direction. Generally, the magnetic intensity or the magnetic induction is measured along the hydrogel axis by Teslameter in experiments [57]. In the present simulation, the measured magnetic intensity decays exponentially away from the magnet surface, namely $H(0, Z) = H_0 e^{-\kappa Z}$, where κ is a characteristic constant for the field distribution, and H_0 is the maximum magnetic intensity at the surface of the magnet. For generating such magnetic field, the magnetic intensity is fitted by a fifth-degree polynomial,

$$H(0, Z) = H_0(aZ^5 + bZ^4 + cZ^3 + dZ^2 + eZ + 1) \tag{26}$$

where *a* ~ *e* are the coefficients of the polynomial, as tabulated in Table 2. Due to the relationship $\mathbf{H} = -\nabla\psi$, the magnetic scalar potential $\psi(0, Z) = P_6(Z)$ is written as a sixth-degree polynomial along the *Z*-axis direction, namely

$$P_6(Z) = H_0\left(\frac{aZ^6}{6} + \frac{bZ^5}{5} + \frac{cZ^5}{4} + \frac{dZ^5}{3} + \frac{eZ^5}{2} + Z + m\right) \tag{27}$$

where *m* is a constant. In the absence of the magnetic hydrogel, the magnetic scalar potential ψ satisfies the Laplace's equation,

$$\frac{1}{R}\frac{\partial}{\partial R}\left(R\frac{\partial \psi}{\partial R}\right) + \frac{\partial^2 \psi}{\partial Z^2} = 0 \tag{28}$$

It is noted that the solution has R^2-symmtry, then the analytical solution is given by

$$\psi(R,Z) = P_6(Z) - \frac{R^2 P_6^{(2)}(Z)}{4} + \frac{R^4 P_6^{(4)}(Z)}{64} - \frac{R^6 P_6^{(6)}(Z)}{2304} \tag{29}$$

which yields the magnetic boundary condition that enforced on the three surrounding edges in Figure 8. The input parameters for the numerical simulation follows those in Subsection 4.1.

Figure 9 shows the deformation contours of the magnetic hydrogel along the field direction at the time $t = 150$ s under different maximum magnetic fields H_0, where hydrogel-magnet distance $L_{hm} = 2.5$mm, the field distribution coefficient $\kappa = 100$, and the black line represents the original geometry of the hydrogel. Without the application of an external magnetic field, the hydrogel elongates homogeneously due to the free swelling governed by the chemical field. The hydrogel is then compressed along the field direction once an external nonuniform magnetic field is exerted. The compression is more significant with the increasing maximum magnetic intensity H_0. When the maximum magnetic intensity H_0 is less than 200kA/m, it is found that the chemical effect is more significant than the magnetic effect. However, when $H_0 = 300$kA/m, the effects of chemical and magnetic effects are almost the same. If the intensity H_0 further increases, the hydrogel displacement becomes negative and the hydrogel length is less than the original one, meaning that the compression along the field direction is larger than the elongation induced by chemical swelling. In addition, it is noted that the deformation pattern under a nonuniform magnetic field is opposite to that under a uniform one shown in Figure 6. From a microscopic point of view, when a nonuniform magnetic field is applied, particle-particle and field-particle interactions concurrently exist, where the former results from the particle

magnetization, and the latter from the magnetic field gradient [51]. The field-particle interaction induces the particle movement towards the location with higher magnetic intensity, and the particle-particle interaction may result in the repelling of the particles. Generally, the deformation induced by the field-particle interaction is much larger than that by particle-particle interaction if a nonuniform magnetic field is imposed, such that the hydrogel contracts along the field direction. However, in a uniform magnetic field, only particle-particle interaction exists, and the mutual repulsion of the particles may stimulate the hydrogel elongation along the field direction.

It is known that the deformation is significantly affected by the magnetic field exerted on the hydrogel, and the magnetic field is mainly controlled by two parameters, namely the maximum magnetic intensity H_0 and the hydrogel-magnet distance L_{hm}. Therefore, Figure 10 is plotted for the influence of the maximum magnetic intensity H_0 on the displacements at the right and upper point of the hydrogel along the field direction and transverse direction against various hydrogel-magnet distances L_{hm} from 2.5 to 15 mm at the time t = 150 s, where the field distribution coefficient $\kappa = 100$. As observed from the figure, with the increase of the distance L_{hm}, the displacement w along the field direction increases and the one u that along the transverse direction decreases. It is known that the hydrogel deformation is dependent on two driving forces. The first one is the chemical swelling force, which contributes to the isotropic expansion of hydrogel, i.e. hydrogel elongation. The second one is the magnetic force, which leads to the compression of the hydrogel along the field direction if the external magnetic field is nonuniform. A longer hydrogel-magnet distance L_{hm} means a lower magnetic field imposed on the hydrogel due to the decay of the magnetic field away from the magnet surface. The compression along

the field direction accordingly decreases, such that the hydrogel deformation induced by the chemical effect becomes larger than that by a magnetic field. In addition, it is found that the displacement *w* is about 0 when the hydrogel-magnet distance $L_{hm} = 2.5\text{mm}$ and the maximum magnetic intensity $H_0 = 300$ kA/m. It is because that the elongation due to the chemical swelling force approaches the compression due to the magnetic force, causing the displacement *w* close to 0. From the inset of Figure 10(a), it is also observed that the displacement *u* at the right and upper point is changed minimally, while the displacement at the right and bottom point is varied significantly, when H_0 increases from 0 to 300 kA/m.

Figure 11 illustrates the effects of the maximum magnetic intensity H_0 and magnetic field distribution coefficient κ on time evolution of the displacements of the magnetic hydrogel along the field and transverse directions, where the hydrogel-magnet distance $L_{hm} = 10\text{mm}$. As seen from the figures, with the increase of the field distribution coefficient κ, the displacement *w* increases significantly, indicating the contribution of the magnetic field on the hydrogel deformation decreases. This is because the larger field distribution coefficient κ means the fast decay of the magnetic field away from the surface of the electromagnet, such that the magnetic field actuated on the hydrogel body is smaller, as also detailed in Figure 13.

Figure 12 is plotted for the hydrogel displacement *w* along the field direction under different magnetic field distribution coefficients κ, where the hydrogel-magnet distance $L_{hm} = 10\text{mm}$, and the external magnetic field is applied at the initial stage, namely $t = 0$. Different from the displacement profile in Figure 11, the hydrogel experiences a gradual increase, where the increasing rate progressively decreases until a steady state is reached.

Moreover, it is found that the hydrogel is compressed when the magnetic field is applied, compared with the case without magnetic field. Furthermore, the compression increases drastically when the magnetic field H_0 increases from 200 to 300 kA/m. It is also noted that the field distribution coefficient κ plays an important role in the displacement profile. It is clear that the compression becomes smaller when the coefficient κ increases from 50 to 125, due to the smaller magnetic field actuated on the hydrogel body. If comparing Figure 11 and 12, it is interesting that the final displacements *w* at $t = 150$ s are the same when the external magnetic is applied at the initial stage or at $t = 100$ s.

As previously stated, the magnetic field distribution shows a significant impact on the response behavior of magnetic hydrogel, such that the distributive profile of non-dimensional magnetic induction B_Z^* and intensity H_Z^* along the vertical line are plotted at the time t = 150 s, when subjected to different field distribution coefficient κ, $L_{hm} = 10$mm, and $H_0 = 300$ kA/m, as shown in Figure 13. It is seen that the magnetic intensity H_Z^* decreases gradually with increasing non-dimensional distance L_Z^*, and it approaches a local minimum at the hydrogel-surrounding interface, where the intensity H_Z^* decreases drastically within a small range of the normalized distance L_Z^*. After that, it drops to another local minimum at the interface, where it rises sharply. Subsequently, the magnetic intensity H_Z^* decreases continuously with L_Z^*. Moreover, the magnetic intensity H_Z^* discontinuously cross the hydrogel-surrounding interface, as also seen from the inset. This is because the hydrogel and its surrounding have different magnetic permeabilities, and the normal part of the magnetic intensity discontinuously goes through the material boundary based on the magnetic boundary condition (21). Additionally, it is also noted that

magnetic intensity H_Z^* deviates from 1, probably due to the pronounced edge effect in the vicinity of the magnetic hydrogel. It is also seen that with the increase of the magnetic field distribution coefficient κ, the corresponding magnetic intensity H_Z^* decreases. It is because that the larger field distribution coefficient κ means the fast decay of the magnetic field away from the surface of the electromagnet, which eventually results in a smaller deformation of the hydrogel. As also observed from the Figure 13(b), it is seen that the magnetic induction B_Z^* is continuously across the hydrogel-magnet interface, which is also line with the requirement on the magnetic boundary condition (21).

4.3. Deformation in a low-frequency alternating magnetic field

Recently, the low-frequency alternating magnetic field is increasingly attracting attentions in biomedical areas [1, 2, 25]. Compared to the previously used static magnetic field, the low-frequency alternating magnetic field may provide a dynamic stimulation environment within controllable magnetic hydrogels in a wireless way. The representative examples include the generation of desired flow patterns in a microfluidic channel for disease diagnosis by Hong *et al.* [25], the dynamic mechanical stimulation on cells for bone generation [1] and for pulsatile drug release [2], and the recent heart repair in rats after myocardial infarction by pulsatile magnetic stimulation on the vagus nerve [58]. Principally, the emerging applications are highly associated with the deformable behavior of the magnetic hydrogel, such that it is necessary to investigate the dynamic response of the hydrogels when subjected to a low-frequency alternating magnetic field. The input parameters follow those in Subsections 4.1 and 4.2, respectively for uniform and nonuniform alternating magnetic fields, where the field period is varied from 4 to 8 s and the magnitude of the magnetic intensity H_0 changes from 0 to 300 kA/m in a period.

Figure 14 shows the time evolution of the hydrogel deformation when a low-frequency alternating uniform magnetic field H_0 is applied at the time $t = 0$ or 100 s, where $\mu_{mr} = 2$ and the red curve represents the time evolution of displacement *w* of hydrogel without magnetic effect. In Figures 14(a) and (b), the external magnetic field is initially applied, the hydrogel experiences a dynamically deformation at a period of 4 and 8 s respectively. The hydrogel displacement *w* is larger than that without the magnetic effect due to the elongation induced by the external magnetic field. In Figures 14 (c) and (d), the dry hydrogel is initially placed in the solvent, and it swells fast within about 10s, followed by a linear and steady increase until $t = 100\text{s}$. Afterwards, an alternating uniform magnetic field is applied and the displacement *w* is also found to be alternating with time. Figure 15 demonstrates the time evolution of the hydrogel deformation when a low-frequency alternating nonuniform magnetic field H_0 is applied at the time $t = 0$ or 100 s, where $\mu_{mr} = 2$, $L_{hm} = 10\text{mm}$ and $\kappa = 100$. In Figures 15(a) and (b), the external magnetic field is initially applied, the hydrogel experiences a dynamically deformation at a period of 4 and 8 s respectively. The hydrogel displacement *w* is smaller than that without the magnetic effect due to the compression from the external magnetic field. In Figures 15 (c) and (d), the hydrogel displacement *w* decreases after 100 s, and it also alternately changes. Moreover, it is noticeable that the period of the displacement *w* is equivalent with that of the magnetic field applied, probably due to the fast responsiveness of the magnetic hydrogels. Therefore, the magnetic field can be tunable remotely in real-time for control of the deformable behavior of the hydrogel.

5. Conclusion

A general thermodynamically consistent framework has been developed for investigation of the deformable behavior of the magnetic hydrogel by considering the coupling effect of the magnetic, chemical, and mechanical fields. Particularly, the magnetic boundary conditions are specified by solving the Laplace's equation for the magnetic scalar potential if a nonuniform magnetic field is imposed. Several case studies are carried out for the impacts of magnetic permeability, field distribution coefficients, and hydrogel-magnet distance on the hydrogel performance, including magnetic field distribution and hydrogel deformation. The numerical results show that the morphology of the hydrogel can be rapidly tuned and the deformation patterns are totally varied when different magnetic field types are applied. Additionally, the hydrogel elongates along the field direction under a uniform magnetic field, while it shrinks when a nonuniform magnetic field is applied. When an alternating uniform magnetic field is imposed, the displacement exhibits a pulsatile variation with the same frequency as the magnetic field applied, demonstrating the fast response of the magnetic hydrogel.

It is known that the microstructures, such as particle size and its arrangement, may play a significant role in the overall macroscopic magnetization, swelling, and the deformation of the magnetic hydrogel. It is worthwhile to formulate a novel microstructure-based magneto-chemo-mechanical model to enrich the theory system of the magnetic soft materials in the future.

Hopefully, the present multiphysics model could provide a theoretical basis to guide the design and optimization of the magnetic hydrogel and its relevant devices, such as magnetic scaffold for dynamic stimulation on cells for bone growth, site-specific drug

delivery and release system for cancer treatment, and microfluidic valves for disease diagnose, where the morphology of the hydrogel is necessarily tailored via a remote way.

References

1. Shou, Y., et al., *Mechano-responsive hydrogel for direct stem cell manufacturing to therapy.* Bioactive Materials, 2023. **24**: p. 387-400.
2. Shou, Y., et al., *Mechano-Activated Cell Therapy for Accelerated Diabetic Wound Healing.* Adv Mater, 2023. **35**(47): p. e2304638.
3. Leganés, J., et al., *Magnetically responsive hydrophobic pockets for on–off drug release.* Materials Today Chemistry, 2022. **23**.
4. Yarali, E., et al., *Magneto‐/electro‐responsive polymers toward manufacturing, characterization, and biomedical/ soft robotic applications.* Applied Materials Today, 2022. **26**.
5. Zhu, H., et al., *Mechanically‐Guided 4D Printing of Magnetoresponsive Soft Materials across Different Length Scale.* Advanced Intelligent Systems, 2021.
6. Manish, V., et al., *Synthesis and characterization of gelatin-based hybrid magnetic hydrogels.* Materials Letters, 2023. **345**.
7. Manish, V., A. Arockiarajan, and G. Tamadapu, *Synthesis, characterization, and modeling of gelatin-based magnetic hydrogel beams.* European Journal of Mechanics - A/Solids, 2024. **106**.
8. Zhan, L., S. Qu, and R. Xiao, *A Review on the Mullins Effect in Tough Elastomers and Gels.* Acta Mechanica Solida Sinica, 2024. **37**(2): p. 181-214.
9. Tang, J., et al., *Shape Morphing of Hydrogels in Alternating Magnetic Field.* ACS Applied Materials & Interfaces, 2019. **11**(23): p. 21194-21200.
10. Liu, X., et al., *Magnetic Living Hydrogels for Intestinal Localization, Retention, and Diagnosis.* Advanced Functional Materials, 2021. **31**(27): p. 2010918.
11. Tang, J., et al., *3D printable, tough, magnetic hydrogels with programmed magnetization for fast actuation.* Journal of Materials Chemistry B, 2021. **9**(44): p. 9183-9190.
12. Hu, W., et al., *Small-scale soft-bodied robot with multimodal locomotion.* Nature, 2018. **554**(7690): p. 81-85.
13. Li, J., et al., *Micro/nanorobots for biomedicine: Delivery, surgery, sensing, and detoxification.* Science Robotics, 2017. **2**(4): p. eaam6431.
14. Tian, Y., et al., *Magnetic-field induced shape memory hydrogels for deformable actuators.* Soft Matter, 2024.
15. Gao, W., et al., *Magnetic Driving Flowerlike Soft Platform: Biomimetic Fabrication and External Regulation.* ACS Applied Materials & Interfaces, 2016. **8**(22): p. 14182-14189.
16. Chen, Z., et al., *Investigation of a new metamaterial magnetorheological elastomer isolator with tunable vibration bandgaps.* Mechanical Systems and Signal Processing, 2022. **170**.
17. Haider, H., et al., *Exceptionally Tough and Notch-Insensitive Magnetic Hydrogels.* Soft Matter, 2015. **11**(42): p. 8253-8261.
18. Cezar, C.A., et al., *Biphasic Ferrogels for Triggered Drug and Cell Delivery.* Advanced Healthcare Materials, 2014. **3**(11): p. 1869-1876.
19. Zrínyi, M., L. Barsi, and A. Büki, *Deformation of Ferrogels Induced by Nonuniform Magnetic Fields.* The Journal of Chemical Physics, 1996. **104**(21): p. 8750-8756.

20. Han, Y., et al., *Magnetostriction and Field Stiffening of Magneto-Active Elastomers.* International Journal of Applied Mechanics, 2015. **7**(1): p. 1550001.
21. Weeber, R., S. Kantorovich, and C. Holm, *Deformation Mechanisms in 2D Magnetic Gels Studied by Computer Simulations.* Soft Matter, 2012. **8**(38): p. 9923-9932.
22. Messing, R., et al., *Cobalt Ferrite Nanoparticles as Multifunctional Cross-Linkers in PAAm Ferrohydrogels.* Macromolecules, 2011. **44**(8): p. 2990-2999.
23. Rutkowski, S., et al., *Magnetically-guided hydrogel capsule motors produced via ultrasound assisted hydrodynamic electrospray ionization jetting.* Journal of Colloid and Interface Science, 2019. **541**: p. 407-417.
24. Rödling, L., et al., *Magnetic Macroporous Hydrogels as a Novel Approach for Perfused Stem Cell Culture in 3D Scaffolds via Contactless Motion Control.* Advanced Healthcare Materials, 2018. **7**(9): p. 1701403.
25. Hong, S., et al., *Magnetoactive sponges for dynamic control of microfluidic flow patterns in microphysiological systems.* Lab on a Chip, 2014. **14**(3): p. 514-521.
26. Lima-Tenório, M.K., et al., *Water transport properties through starch-based hydrogel nanocomposites responding to both pH and a remote magnetic field.* Chemical Engineering Journal, 2015. **259**(0): p. 620-629.
27. Dorfmann, A. and R.W. Ogden, *Some Problems in Nonlinear Magnetoelasticity.* Zeitschrift für angewandte Mathematik und Physik, 2005. **56**(4): p. 718-745.
28. Dorfmann, A. and R.W. Ogden, *Nonlinear magnetoelastic deformations.* Quarterly Journal of Mechanics and Applied Mathematics, 2004. **57**(4): p. 599-622.
29. Nedjar, B., *A Theory of Finite Strain Magneto-Poromechanics.* Journal of the Mechanics and Physics of Solids, 2015. **84**: p. 293-312.
30. Kadapa, C. and M. Hossain, *A unified numerical approach for soft to hard magneto-viscoelastically coupled polymers.* Mechanics of Materials, 2022. **166**.
31. Garcia-Gonzalez, D. and M. Hossain, *A microstructural-based approach to model magneto-viscoelastic materials at finite strains.* International Journal of Solids and Structures, 2021. **208-209**: p. 119-132.
32. Garcia-Gonzalez, D. and M. Hossain, *Microstructural modelling of hard-magnetic soft materials: Dipole–dipole interactions versus Zeeman effect.* Extreme Mechanics Letters, 2021. **48**.
33. Weeber, R., S. Kantorovich, and C. Holm, *Ferrogels Cross-Linked by Magnetic Nanoparticles—Deformation Mechanisms in Two and Three Dimensions Studied by Means of Computer Simulations.* Journal of Magnetism and Magnetic Materials, 2015. **383**(0): p. 262-266.
34. Pessot, G., et al., *Towards a Scale-Bridging description of Ferrogels and Magnetic Elastomers.* Journal of Physics: Condensed Matter, 2015. **27**(32): p. 325105.
35. Filipcsei, G. and M. Zrínyi, *Magnetodeformation Effects and the Swelling of Ferrogels in a Uniform Magnetic Field.* Journal of Physics: Condensed Matter, 2010. **22**(27): p. 276001.
36. Liu, Q., et al., *A multiphysics model of magnetic hydrogel under a moving magnet for targeted drug delivery.* International Journal of Mechanical Sciences, 2022. **215**: p. 106963.

37. Liu, Q., H. Li, and K.Y. Lam, *Modeling of a fast-response magnetic-sensitive hydrogel for dynamic control of microfluidic flow.* Physical Chemistry Chemical Physics, 2019. **21**(4): p. 1852-1862.
38. Garcia-Gonzalez, D. and C.M. Landis, *Magneto-diffusion-viscohyperelasticity for magneto-active hydrogels: Rate dependences across time scales.* Journal of the Mechanics and Physics of Solids, 2020. **139**: p. 103934.
39. Liu, Q., et al., *Multiphysics modeling of responsive deformation of dual magnetic-pH-sensitive hydrogel.* International Journal of Solids and Structures, 2020. **190**: p. 76-92.
40. Liu, Q., et al., *Transient modeling of magneto-chemo-electro-mechanical behavior of magnetic polyelectrolyte hydrogel.* Mechanics of Materials, 2021. **155**: p. 103783.
41. Hu, J., et al., *Inhomogeneous large deformation of magneto-thermal sensitive hydrogel-based composite structures.* Mechanics of Advanced Materials and Structures, 2023: p. 1-9.
42. Han, Y., W. Hong, and L. Faidley, *Coupled Magnetic Field and Viscoelasticity of Ferrogel.* International Journal of Applied Mechanics, 2011. **03**(02): p. 259-278.
43. Pelteret, J.-P., et al., *Computational electro- and magneto-elasticity for quasi-incompressible media immersed in free space.* International Journal for Numerical Methods in Engineering, 2016. **108**: p. 1307–1342.
44. Wei, H., et al., *Magnetoactive Millirobots with Ternary Phase Transition.* ACS Appl Mater Interfaces, 2024.
45. Emi, T., et al., *Pulsatile Chemotherapeutic Delivery Profiles Using Magnetically Responsive Hydrogels.* ACS Biomaterials Science & Engineering, 2018.
46. Birgersson, E., H. Li, and S. Wu, *Transient Analysis of Temperature-sensitive Neutral Hydrogels.* Journal of the Mechanics and Physics of Solids, 2008. **56**(2): p. 444-466.
47. Hong, W., et al., *A Theory of Coupled Diffusion and Large Deformation in Polymeric Gels.* Journal of the Mechanics and Physics of Solids, 2008. **56**(5): p. 1779-1793.
48. Coussy, O., L. Dormieux, and E. Detournay, *From Mixture Theory to Biot's Approach for Porous Media.* International Journal of Solids and Structures, 1998. **35**(34–35): p. 4619-4635.
49. Zheng, P. and K. Zhang, *On the effective stress law and its application to finite deformation problems in a poroelastic solid.* International Journal of Mechanical Sciences, 2019. **161-162**: p. 105074.
50. Gurtin, M.E., E. Fried, and L. Anand, *The Mechanics and Thermodynamics of Continua*. 2010, Cambridge, U.K.: Cambridge University Press.
51. Liu, Q., H. Li, and K.Y. Lam, *Development of a Multiphysics Model to Characterize the Responsive Behavior of Magnetic-Sensitive Hydrogels with Finite Deformation.* The Journal of Physical Chemistry B, 2017. **121**(22): p. 5633-5646.
52. Flory, P.J., *Thermodynamics of High Polymer Solutions.* The Journal of Chemical Physics, 1942. **10**(1): p. 51-61.
53. Liu, Y., H. Zhang, and Y. Zheng, *A multiplicative finite element algorithm for the inhomogeneous swelling of polymeric gels.* Computer Methods in Applied Mechanics and Engineering, 2015. **283**: p. 517-550.

54. Wei, G., L. Meie, and Z. Jinxiong, *Modeling programmable deformation of self-folding all-polymer structures with temperature-sensitive hydrogels.* Smart Materials and Structures, 2013. **22**(11): p. 115028.
55. Bouklas, N., C.M. Landis, and R. Huang, *A Nonlinear, Transient Finite Element Method for Coupled Solvent Diffusion and Large Deformation of Hydrogels.* Journal of the Mechanics and Physics of Solids, 2015. **79**: p. 21-43.
56. Afkhami, S., et al., *Field-induced Motion of Ferrofluid Droplets through Immiscible Viscous Media.* Journal of Fluid Mechanics, 2008. **610**: p. 363-380.
57. Zrínyi, M., et al., *Direct Observation of Abrupt Shape Transition in Ferrogels Induced by Nonuniform Magnetic Field.* Journal of Chemical Physics, 1997. **106**(13): p. 5685-5692.
58. Bao, S., et al., *Rapid improvement of heart repair in rats after myocardial infarction by precise magnetic stimulation on the vagus nerve with an injectable magnetic hydrogel.* Nanoscale, 2023. **15**(7): p. 3532-3541.

List of tables

List of figures

Table 1. Solution procedure for the numerical simulation.

Step I. Inputting the physical and chemical parameters, as well as the initial and boundary conditions;
Step II. Calculating the initial variables for time step $t+\Delta t$;
Step III. Coupled solution for time step $t+\Delta t$;
A. Solving the magnetic and chemical fields at the coupled iteration step $n+1$:
a. Estimating solution $\psi^{new}=\psi^{n}\ \ C_s^{new}=C_s^{n}$;
b. Calculating the Jacobian matrix and right-hand side;
c. Imposing the Dirichlet and /or Neumann boundary conditions;
d. Solving $\Delta\psi$, ΔC_s;
e. Updating the solution, $\psi^{new}\leftarrow\psi^{old}+\Delta\psi$, $C_s^{new}\leftarrow C_s^{old}+\Delta C_s$;
f. Checking the convergence criterion, if not met, go to Step A (b);
B. Calculating the magnetic intensity by Equation (2)
C. Solving the mechanical field at the coupled iteration step $n+1$:
a. Estimating solution $u^{new}=u^{n}$;
b. Calculating the Jacobian matrix and right-hand side;
c. Imposing the Dirichlet and /or Neumann boundary conditions;
d. Solving Δu ;
e. Updating the solution, $u^{new}\leftarrow u^{old}+\Delta u$;
f. Checking the convergence criterion, if not met, go to Step C (b);
Step IV. Updating displacement, counter, and time by $u^{n+1}\leftarrow u^{new}$, $n\leftarrow n+1$, $t\leftarrow t+\Delta t$;
Step V. Output the results. If the simulation is not completed, go to Step II.

Table 2. Coefficients of the fifth polynomial when the field distribution coefficient κ is changed.

	$\kappa=50$	$\kappa=75$	$\kappa=100$	$\kappa=125$
a	-276940.0	-818971.2	-1489374.4	-2144428.8
b	98357.4	265724.5	461956.78	648202.2
c	-14379.1	-33866.8	-55024.6	-74301.5
d	1122.9	2154.3	3155.2	4015.0
e	- 49.1	-70.6	- 88.3	-102.3

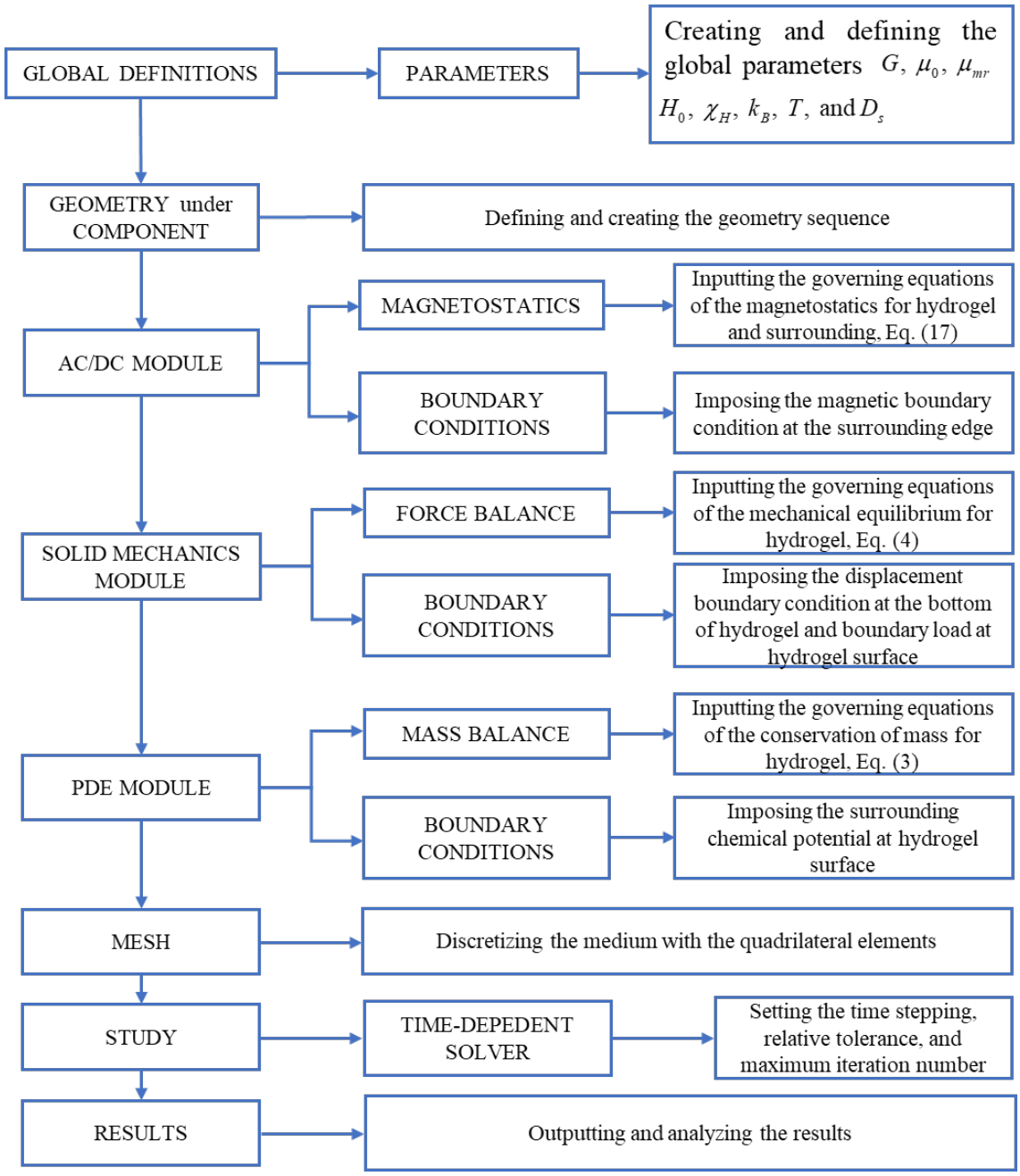

Figure 1. Flow of the present numerical implementation and simulation.

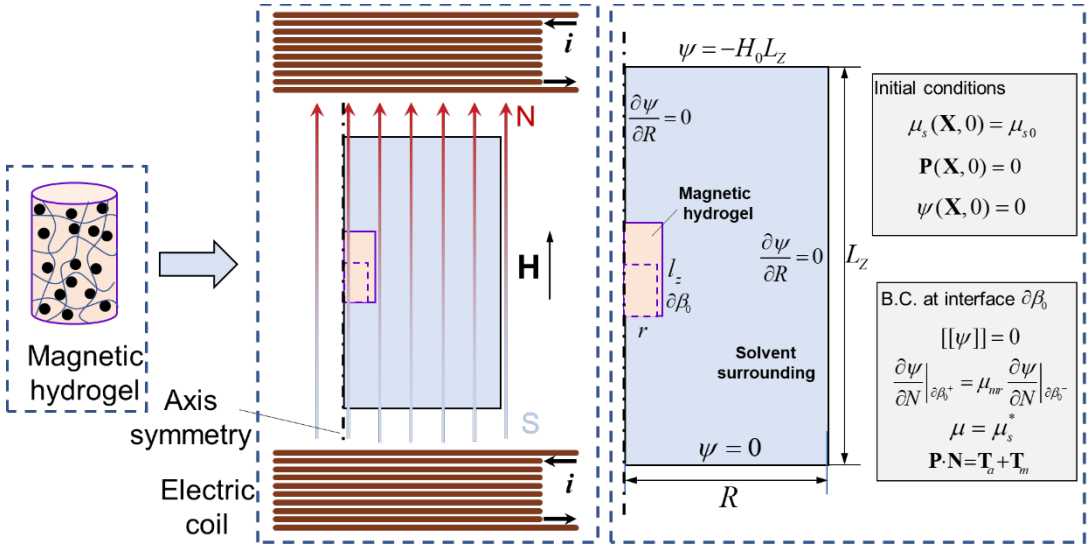

Figure 2. Schematic of the magnetic hydrogel placed in a solvent surrounding and subjected to an externally applied uniform magnetic field created by two pairs of electromagnets.

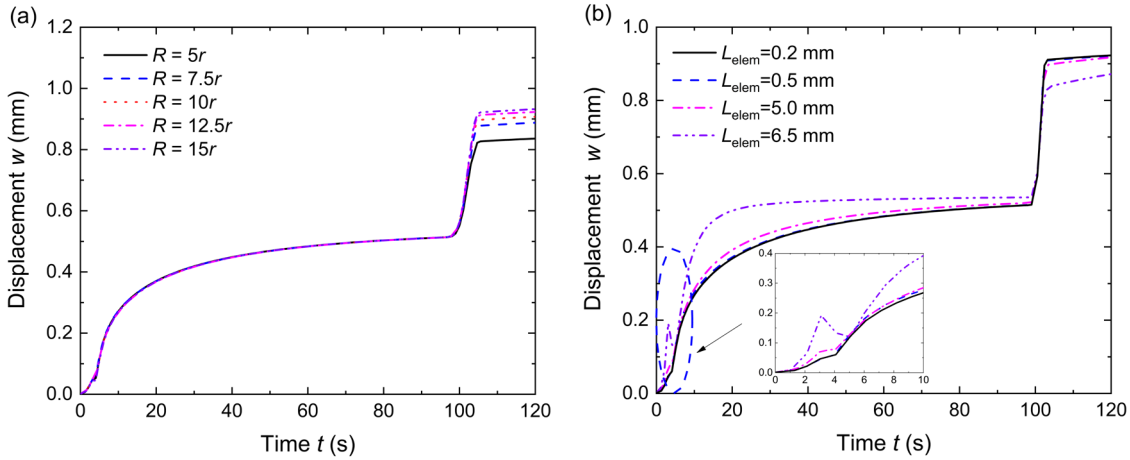

Figure 3. Identifications of the simulated surrounding domain and the element size by the mesh independent study. (a) Influence of surrounding size R on time evolution of displacement along the field direction w. (b) Influence of maximum element size L_{elem} on time evolution of displacement w.

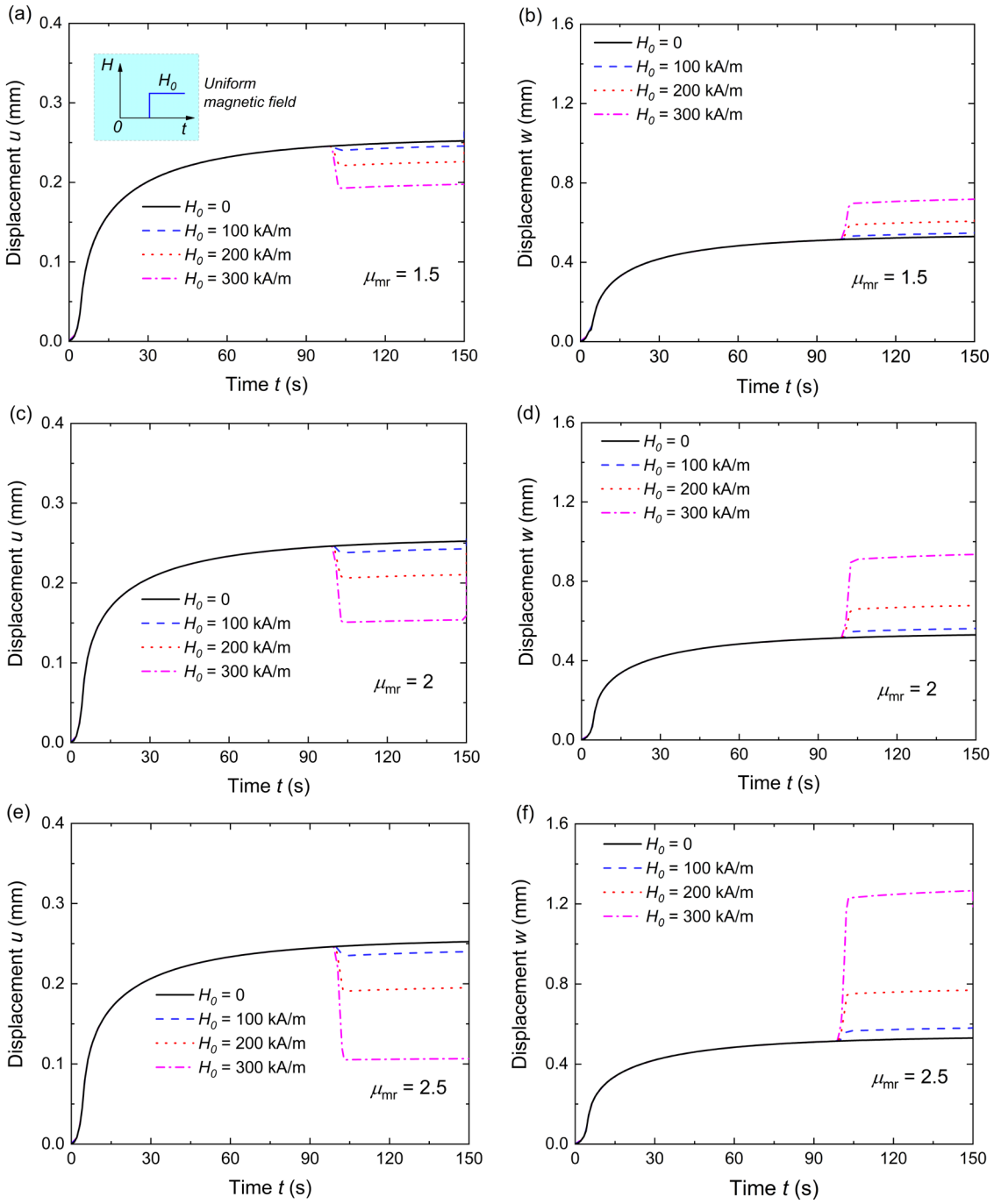

Figure 4. Time evolution of the displacements of the magnetic hydrogel along the transverse and field directions under different magnetic intensities H_0 and permeabilities μ_{mr}, where the hydrogel swells first and then the external magnetic field is applied to deform the hydrogel.

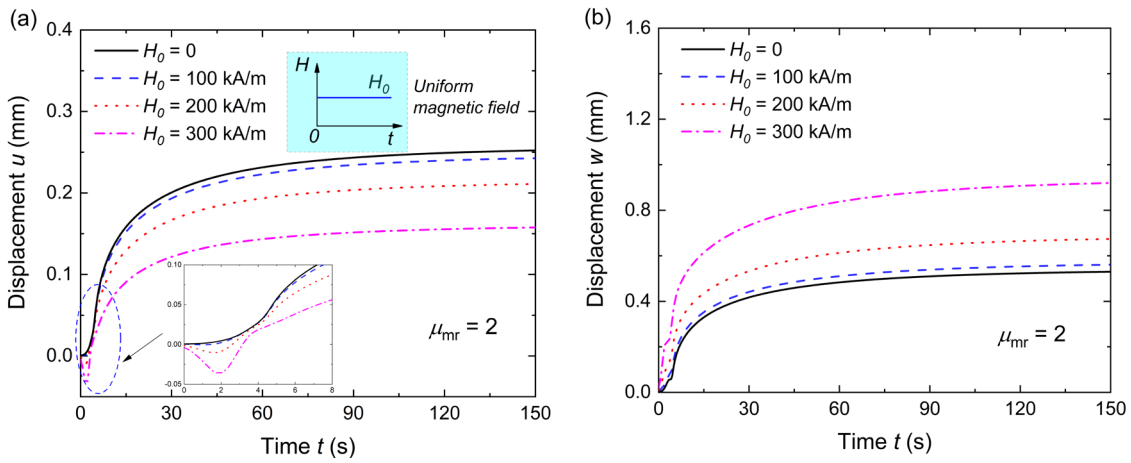

Figure 5. Time evolution of the displacements of the magnetic hydrogel along the transverse and field directions under different magnetic intensities H_0, where the external magnetic field is applied at the initial stage.

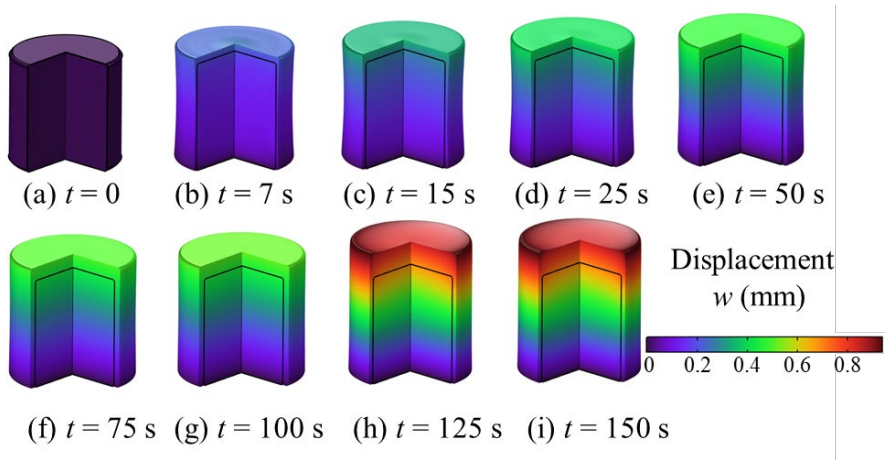

Figure 6. Contours of the deformation of the magnetic hydrogel when $H_0 = 300\text{kA/m}$ and $\mu_{mr} = 2$.

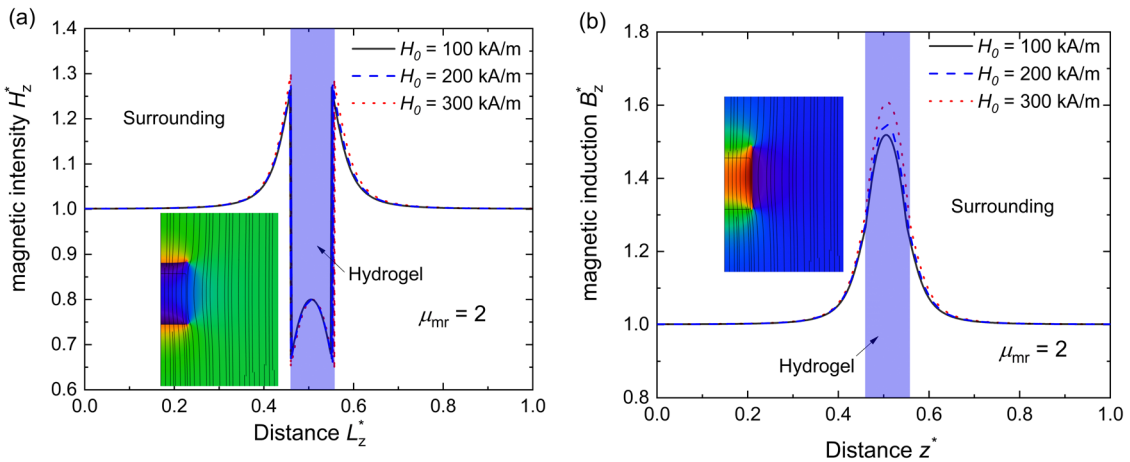

Figure 7. Influence of external magnetic field H_0 on the distributions of (a) non-dimensional magnetic induction B_Z^* and (b) intensity H_Z^* along the vertical line $r = 0$, when the time $t = 150$ s.

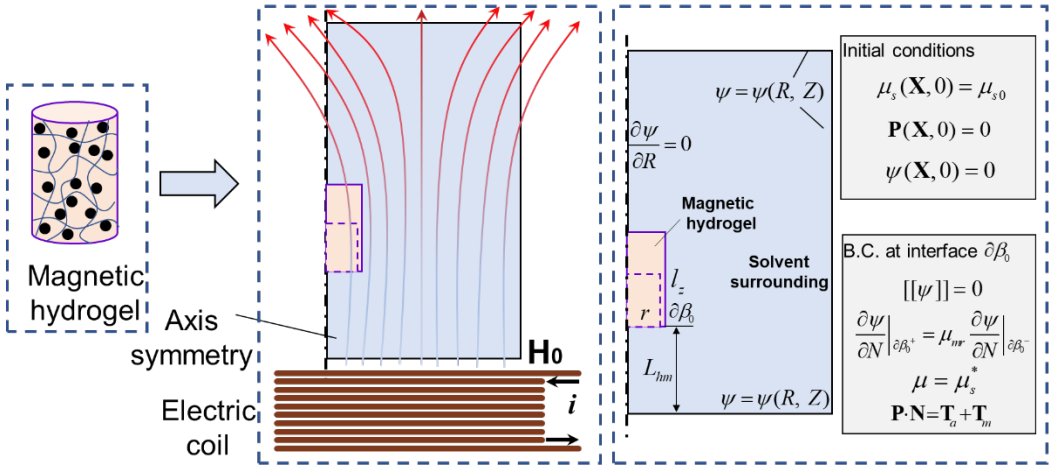

Figure 8. Schematic of the magnetic hydrogel that is placed in a solvent surrounding when subjected to a nonuniform magnetic field.

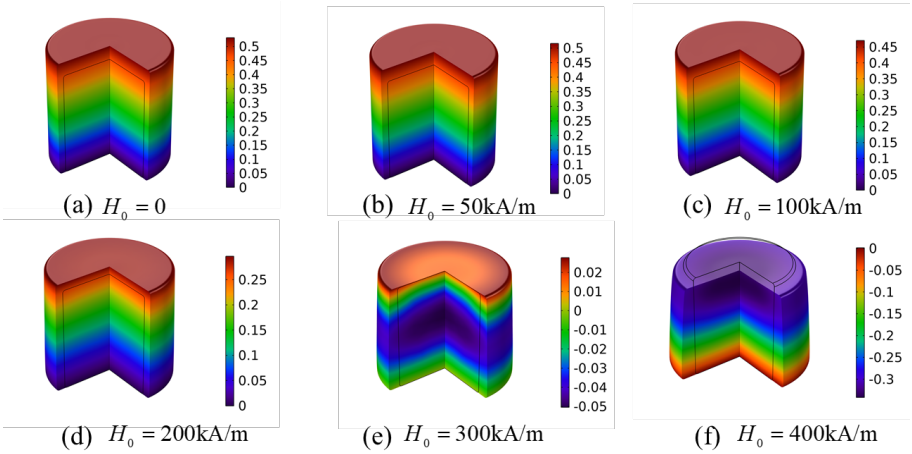

Figure 9. Deformation contours of the magnetic hydrogel under different maximum magnetic intensities H_0 from 0 to 400 kA/m, where hydrogel-magnet distance $L_{hm} = 2.5\text{mm}$, the field distribution coefficient $\kappa = 100$, and the black line represents the original geometry of the hydrogel.

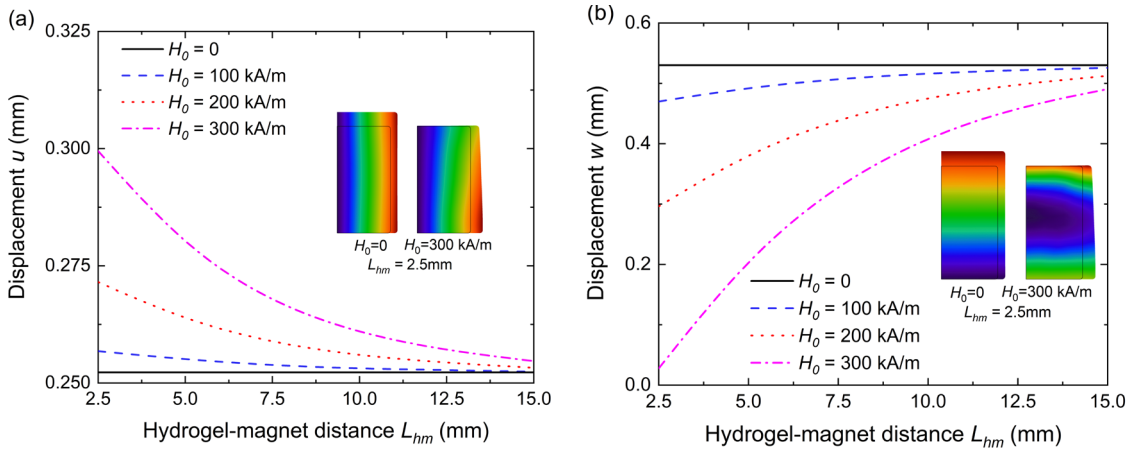

1 **Figure 10**. Influence of maximum magnetic intensity H_0 on variation of the displacements
2 of the magnetic hydrogel along the field and transverse directions respectively, against
3 varying hydrogel-magnet distance L_{hm} from 2.5 to 15 mm at the time t = 150 s, where the
4 field distribution coefficient $\kappa = 100$.
5

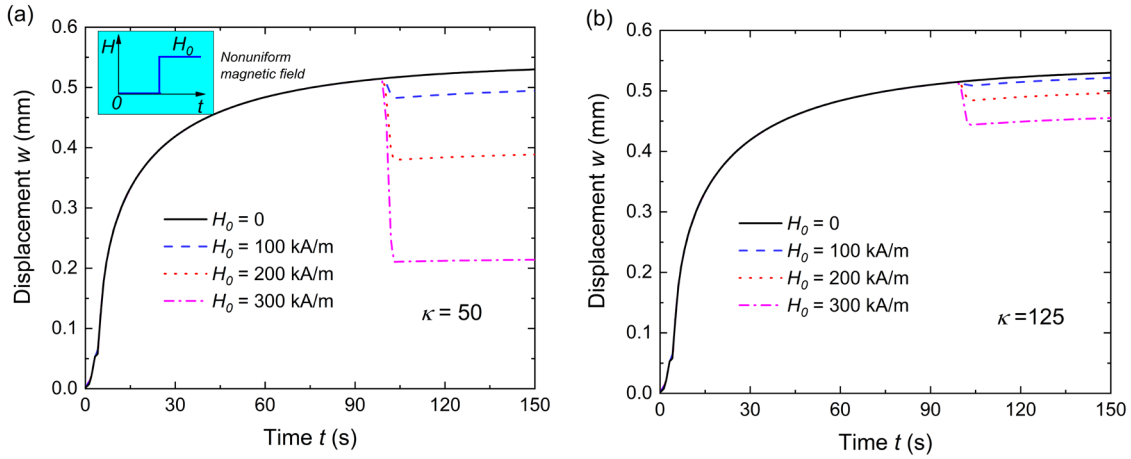

6 **Figure 11**. Influence of maximum magnetic intensity H_0 on time evolution of the
7 displacement of the magnetic hydrogel along the field direction under different field
8 distribution coefficient κ, where the hydrogel-magnet distance $L_{hm} = 10$mm and the
9 external magnetic field is applied at the time t =100 s.
10

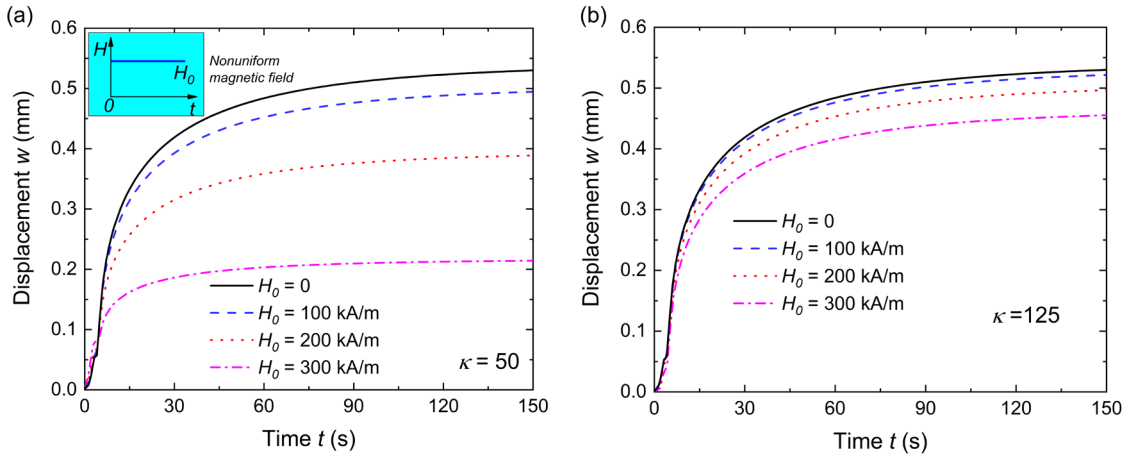

Figure 12. Influence of maximum magnetic intensity H_0 on time evolution of the displacement of the magnetic hydrogel along the field direction under different field distribution coefficient κ, where $L_{hm} = 10\text{mm}$ and the external magnetic field applied at the initial stage.

1

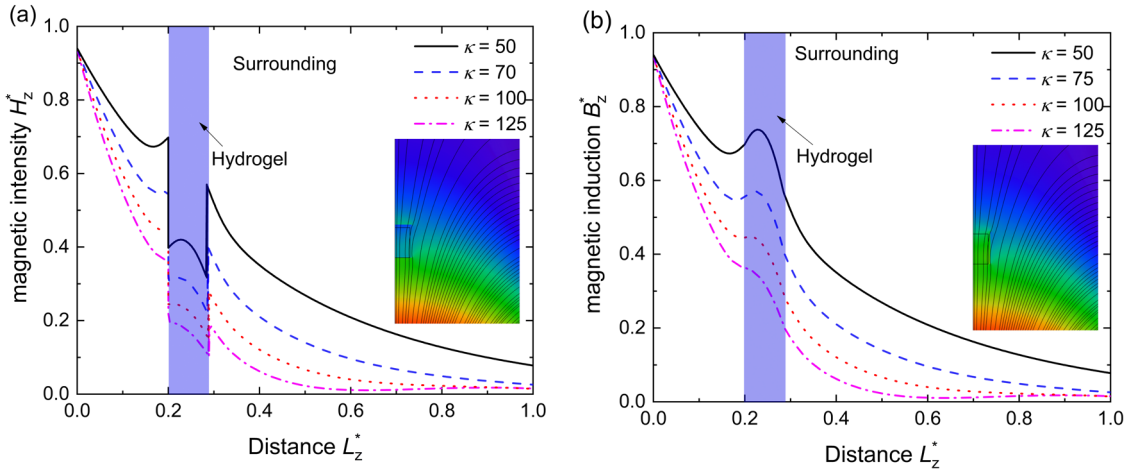

2 **Figure 13**. Influence of field distribution coefficient κ on the distributions of (a) non-

3 dimensional magnetic intensity H_Z^* and (b) induction B_Z^* along the vertical line $r = 0$,

4 where the hydrogel-magnet distance $L_{hm} = 10\text{mm}$.

5

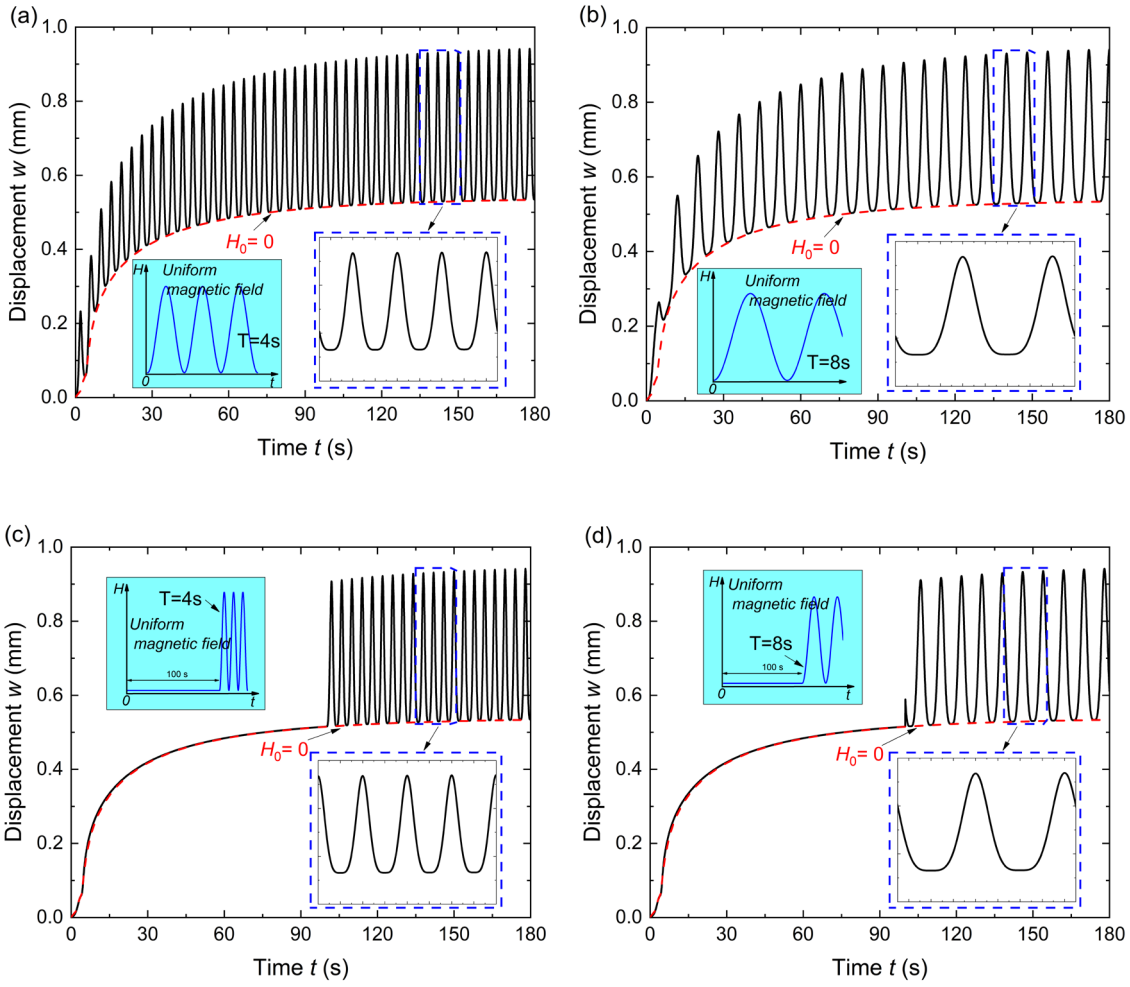

Figure 14. Influence of the low-frequency alternating uniform magnetic field on the displacement *w* of the magnetic hydrogel along the field direction, where $H_0 = 300$ kA/m .

1

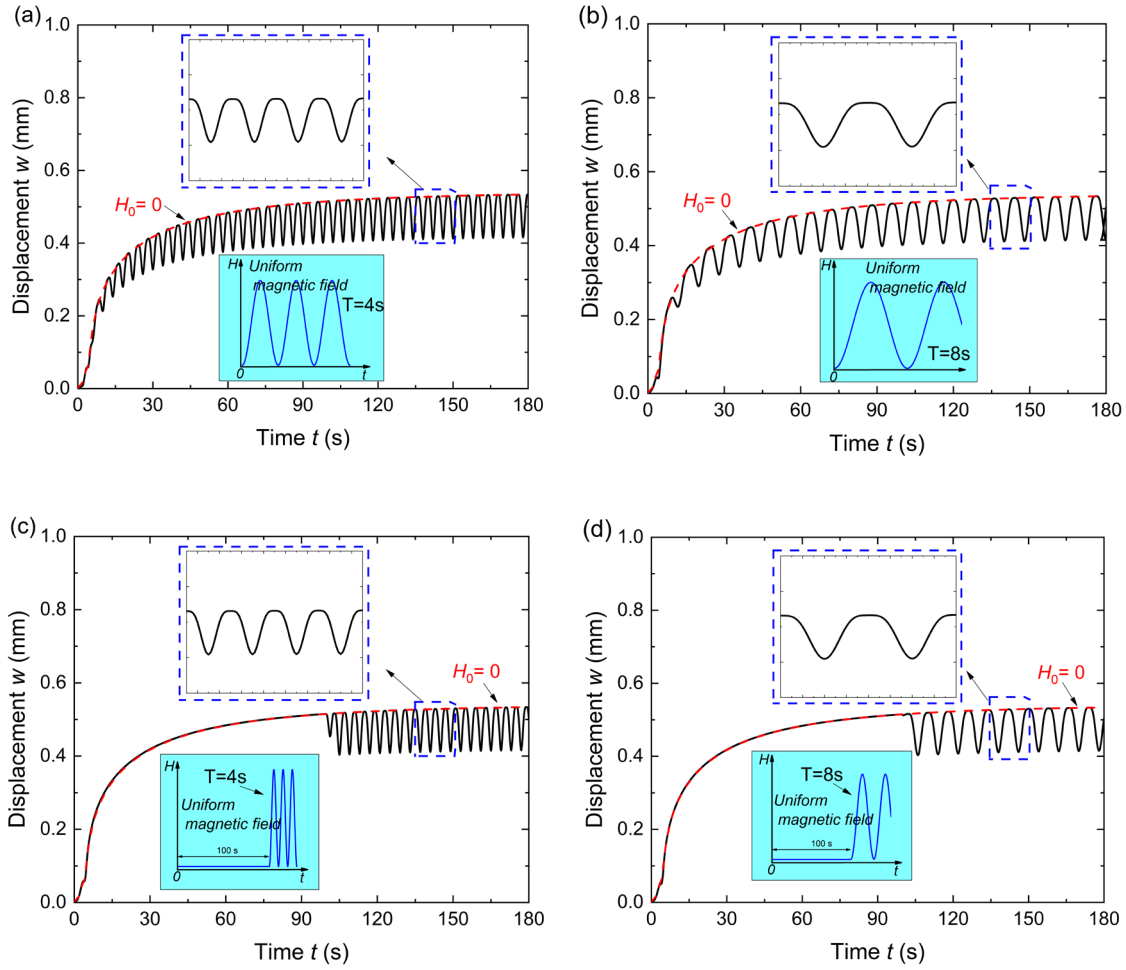

2 **Figure 15**. Influence of the low-frequency alternating nonuniform magnetic field on the

3 displacement *w* of the magnetic hydrogel along the field direction, where $H_0 = 300$ kA/m

4 , $\kappa = 100$, and $L_{hm} = 10\text{mm}$.

5